

Alignment survey results for the Electrostatic Quadrupole System of the Muon g-2 Experiment

M. Kargantoulakis¹

¹Fermilab
ekargian@fnal.gov

March 26, 2019

Abstract

This note describes the motivation and efforts to determine the quality of alignment of the Electrostatic Quadrupole System. Several independent surveys were performed, and their combination provides the best determination of the location of the Electrostatic Quadrupole System plates, as well as an estimation of their uncertainty.

Contents

1	Introduction	3
2	Installation and survey	5
2.1	Capacitec and micrometer surveys	5
2.2	Laser alignment system survey before installation	5
3	EQS location inside the storage ring	6
3.1	Global analysis	7
3.2	Location of individual plates	9
3.2.1	Large Q4S inner and outer plate displacements	11
4	In situ surveys of quadrupole plates	12
4.1	Through-flange extension probe	14
4.1.1	Extension probe dataset	16
4.2	Proximity sensors mounted on the trolley	21
4.2.1	Scraping of sensors in vacuum region	23
4.2.2	The VCNL4010 dataset	23
5	Location and uncertainty of quadrupole plates	31

6 Conclusion	33
Appendices	34
A Survey of kicker plates	34

1 Introduction

The g-2 storage ring acts as a weak-focusing betatron, with the vertical focusing provided by the Electrostatic Quadrupole System (EQS) [1]. A pure quadrupole electric field provides a linear restoring force in the vertical direction, and the combination of the (defocusing) electric field and the central (dipole) magnetic field provides a net linear restoring force in the radial direction.

Ideally, the EQS plates should fill as much of the azimuth as possible, but space is required for the inflector and kicker magnets, fiber monitors, and field trolley garage. Both BNL and Fermilab Muon g-2 experiments chose a symmetric configuration which places the quadrupoles in four distinct regions, Q1-Q4, as shown in Fig. 1. Gaps at 0° and 90° for the inflector and kicker magnets, along with empty gaps at 180° and 270° provide a four fold symmetry.

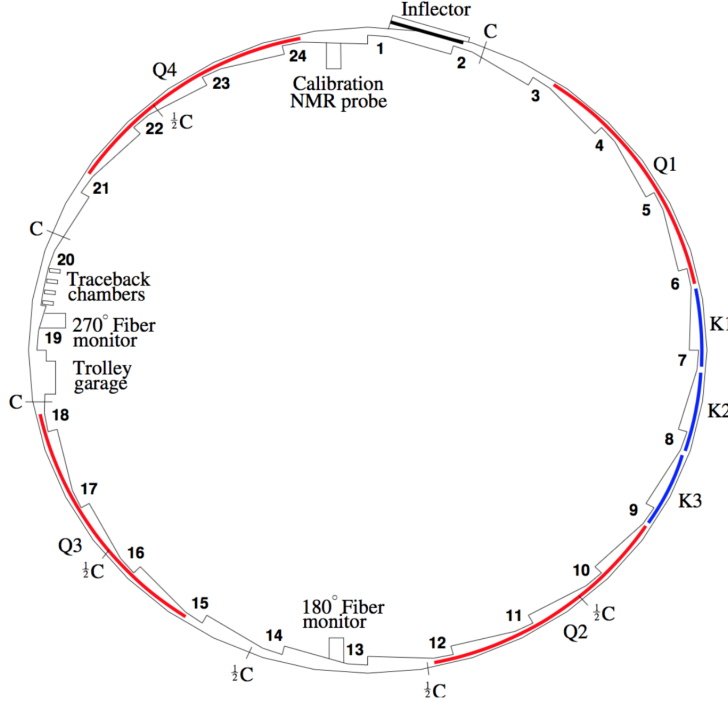


Figure 1: A schematic overview of the $g-2$ storage ring. The locations of the 4 EQS sections are marked in red.

Overall the electrodes occupy 43% of the total circumference. The four-fold symmetry keeps the variation in the beta function small, which minimizes beam breathing and improves the muon orbit stability. Each quad segment consists of a short quad with azimuthal coverage of 13° and a long quad of 26° , for two reasons: 1) to make every quadrupole half-segment independent of others,

facilitating their development, testing, etc., and 2) to reduce the extent of low-energy electron trapping. Therefore, there are two high-voltage vacuum-to-air interfaces for each quadrupole segment [2].

A schematic representation of a cross-section of the electrostatic quadrupoles is shown in Fig. 2 with the various dimensions indicated. The four aluminum plates are symmetrically placed around the muon storage region, with 10 cm between opposite plates.

Plate alignment

Any misalignment of ESQ plates translates to a modification of their E-field and thus a deviation from ideal storage conditions, inducing perturbations to the orbit of stored muons and systematic shifts to the experimental measurement. Therefore good knowledge of the location of the ESQ plates is necessary for reliable operation and analysis.

The placement accuracy specifications for the EQS plates are determined by the estimated effects of a potential misplacement on the electric field and the muon orbit. For the vertically-installed side electrodes (inner and outer plates) the average deviation from the ideal position should be within 0.75 mm. For the top and bottom plates the average deviation should be within 0.5 mm. These are the same specifications as were used E821, and are retained for the Fermilab Muon g-2 Experiment.

We further state that the standard deviation (RMS) over a short quad length should be less than ± 0.75 mm for the inner/outer plates, and less than ± 0.5 mm for the top/bottom plates. The deviation from the ideal location should not exceed ± 2 mm at any point [3], a specification that is important also for safe clearance from the NMR trolley.

To give a scale of the potential effect, the size of the E-field correction can be expressed as [4]

$$\frac{\Delta\omega_\alpha}{\omega_\alpha} = \frac{2\beta^2 n(1-n)}{R_0^2} (\langle x_{eq}^2 \rangle + \langle x_{eq} \rangle \frac{h}{1-n}), \quad (1)$$

where $\langle x_{eq} \rangle$ is the average offset of the equilibrium orbit from the center of the quadrupole potential, and h is the displacement of the center of the quadrupole

potential. Given the large offset of the equilibrium orbit in Run 1 of approximately 5 mm, a 1 mm displacement of the quadrupole plates can shift the correction by approximately 20 ppb. An independent tracking study [5] finds roughly 10-25 ppb shift in the E-field correction per mm of quad displacement, confirming the size of the effect. Given the linear coupling with the offset in the equilibrium radius distribution, a 1 mm uncertainty in the quadrupole potential center would similarly contribute \sim 20 ppb of uncertainty to the correction. Therefore sub-mm precision is desired in our knowledge of the plate location.

2 Installation and survey

This section describes measurements and surveys of the electrodes location, with the plates mounted on the cage but before the cages were inserted into vacuum chambers.

2.1 Capacitec and micrometer surveys

The initial survey of the quad plates position employed Capacitec [6] sensors with HPB button probes, non-contact and highly sensitive to displacements over a thin gap based on a capacitive measurement. The probes are connected through cables to Series 4000 amplifying readout electronics. The Capacitec sensors offered a very good solution for measuring plate location inside their cage, before the cage was installed in vacuum chambers. The sensors were mounted on a trolley and sampled the plates' location. A relatively small range of linear operation was found within 0-3 mm, but that was enough for reliable measurement. The initial survey is described in [7]. Unfortunately, it looks like the Capacitec measurement is not fully stable and repeatable, so it was eventually abandoned.

Based on the Capacitec measurements, some adjustments of the plates was attempted as they were mounted on the standoffs, to minimize deviations from their design location. The final alignment was achieved by using the micrometer tools designed by J. Grange and H. Nguyen. To slightly adjust the position locally, a half or full washer was added between the standoff and the plate. The procedures to align the plates during installation are described in [8]

2.2 Laser alignment system survey before installation

After the plates were installed in the cages, as closely to their ideal position as possible, their position was determined by the Alignment and Metrology Department (AMD) using a handheld 3D laser scanning system, the API I-Scan II [9]. The system performs dynamic non-contact scanning of the plate surface, achieving 50-100 μm resolution.

Measurement with the laser scanner can be seen in Fig. 3. The plates surface outside the cage is sampled, then under assumption of constant and ideal plate thickness, the location of the inner surface is extracted. Tens or hundreds of

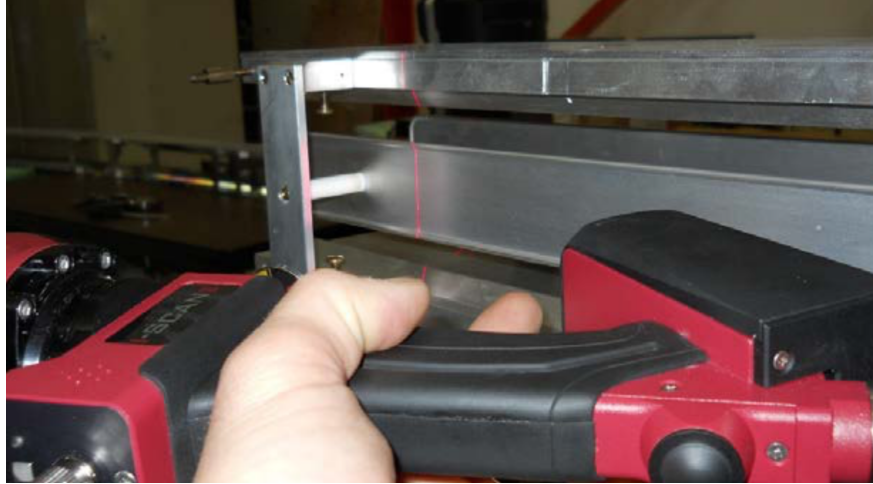


Figure 3: AMD measurement with the handheld laser scanning system.

thousands of points were scanned per plate, providing very detailed information of the plate surface.

An example of data from a sampled plate is shown in Fig. 4. The high-density blue data come from the laser scan, and the hand-held micrometer measurements are shown in red for comparison. The agreement is very good. The vertical axis is distance in mm from the center of the storage ring. Note that the plates here are not installed inside a vacuum chamber and not yet located inside the ring. The AMD group used fiducial markers located onto the cage, and then expressed the laser scan measurements in storage ring coordinates under the assumption that the cage will be located in its ideal position. The horizontal axis in the figure is length along the plate. The regions where the vertical RMS of the laser data grows suggest a tilt of the plate, *i.e.* the plate's radial position varies from top to bottom.

3 EQS location inside the storage ring

After installation and initial survey of the plates with respect to the cage, the cages were inserted to the vacuum chambers. The AMD group surveyed the vacuum chambers and was able to express the EQS plates location in storage ring coordinates. The assumption is made that the cage remained perfectly rigid during insertion to the chamber. Then the existing laser scan data with respect to the cage can be expressed in real storage ring coordinates.

An initial survey was used to adjust the radial position of the vacuum chambers in order to optimize the location of the quad plates and bring them as close to ideal as possible. A vertical adjustment of the chambers was not possible, so only the radial location was optimized. After this corrective motion, the final

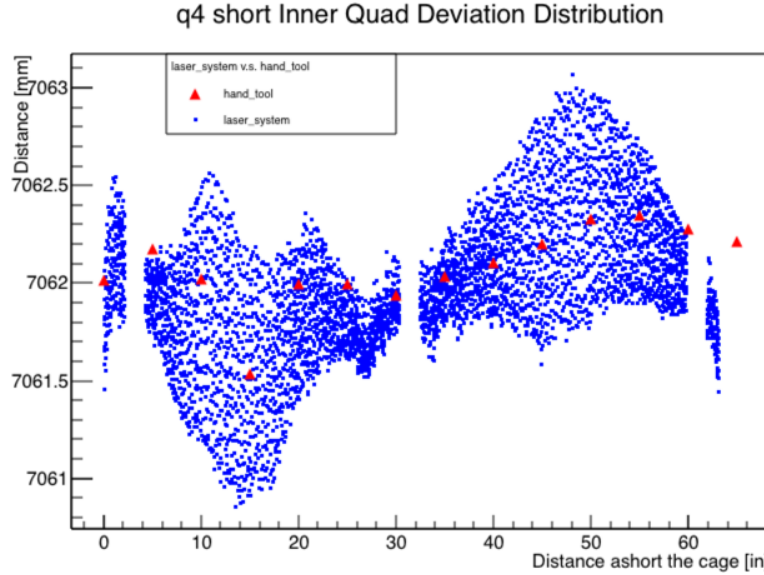


Figure 4: Alignment data on the Q4S inner plate. Blue is from the AMD laser scan, red is from the hand-held micrometer tool.

survey of the chambers gives the location of the EQS plates. Data from this survey can be found at [10] and we will refer to it as the laser scan dataset. Important details therein went without analysis for some time. We examine this rich dataset in this section.

3.1 Global analysis

In the global analysis of [10] by Horst Friedsam, the head of the Alignment and Metrology Department, all 8 EQS plates of a given type (inner, outer, top, or bottom) were fit globally, including all Q1-Q4 regions around the ring. The inner plates (and separately the outer) were fit globally to a single cylindrical surface. The top (and bottom) plates were fit globally to a plane surface. An example of such a fit is shown for the top plates at Fig. 5.

The results from these global fits are given in Table 1. The average vertical location of the top and bottom plane surfaces are within 0.4 mm from the design value. The average radius of the global inner and outer cylindrical surfaces are within 0.3 mm from ideal. As noted in the original analysis, the RMS of the residuals of these global fits is significant. As can be seen from 5, this is due to large residuals on individual plates. To gain more insight, studies on individual plates are required.

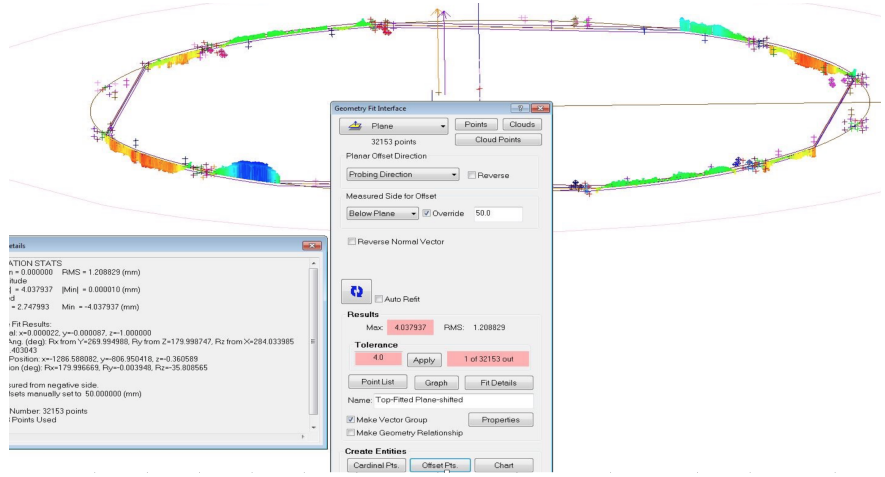


Figure 5: Screen capture from Horst's analysis. A global fit is performed of all 8 top plates around the ring to a single plane surface. Fit residuals are plotted here.

Table 1: Global fit locations of EQS plates and offsets from ideal. All values in mm.

	Global fit	Ideal value	Offset from ideal	RMS
Top plate, vertical location	49.597	50	0.403	1.209
Bottom plate, vertical location	50.223	50	-0.223	1.140
Inner plate, radial location	7061.74	7062	0.26	0.77
Outer plate, radial location	7161.77	7162	0.231	1.11

Q1S bottom plate z:r:theta

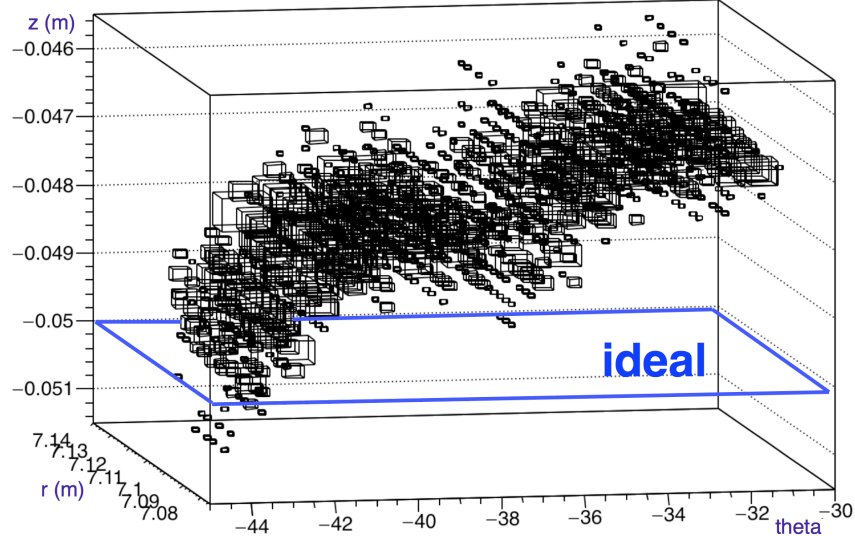


Figure 6: AMD data on the bottom plate of the short Q1 quad, plotted in 3 dimensions: vertical z , radial r , and azimuth. The ideal position of the plate is marked in blue at $z=-0.05$ m.

3.2 Location of individual plates

Examining the data on individual plates, significant deviations from their ideal location are discovered, in many cases even outside specification [11]. In Fig. 6 the AMD data on the bottom plate of the short Q1 quad are plotted 3-dimensionally. A significant deviation from the ideal position is apparent, along with a non-linear azimuthal dependence of the vertical location.

Another visualization is given in Fig. 7, again using the Q1 short plates as example. Here the plates are drawn in two dimensions, with color coding for the coordinate of most interest: vertical for the top and bottom plates, radial for the inner and outer. The red bands next to the color code bars mark the regions that are outside the 2 mm spec. Note the large radial variations on Q1 short outer plate. This is the plate constructed from aluminized Mylar. As the Mylar stretches it forms waves, and the laser scan provides a unique depiction of that. The color-coded plots for all quads can be found in [11].

Having noted some significant deviations from the 2 mm requirement on some locations, as well as some azimuthal and vertical dependence which suggests a tilt in the plates, the average deviations of each plate from their ideal position are listed in Table 2. The cells marked in red have severe deviations from the specification of 0.5 mm (0.75 mm) of average displacement per top/bottom (inner/outer) plate. Those marked in yellow also exhibit concerningly large

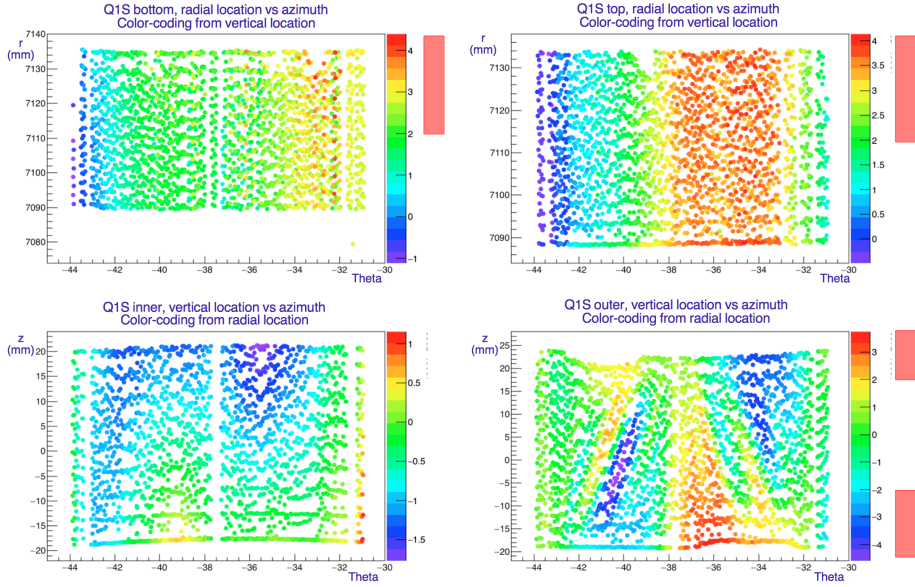


Figure 7: AMD data on all 4 Q1 short plates. The top two plots are radial location versus azimuth for the bottom and top plates, with the color-coding marking vertical location. The bottom two plots are vertical location versus azimuth for the inner and outer plates, with the color-coding marking radial location. In each case the color-coded coordinate is expressed in mm of deviation from the ideal position.

deviations. The rest are mostly within the specification, or not significantly outside it.

The deviations tend to be of opposite sign on short and long plates of the same quad, especially on the top and bottom plates of Q1 and Q3. This is also evident in more detail in Fig. 5. A potential tilt of the installed cages or chambers that contain these quads could be the reason for this. The opposite deviations cancel and result in a small overall deviation of the top and bottom plates in the global fit, hence the global deviations are small even though they can be quite large on individual plates. This also explains the large RMS of the global fits in Table 1.

Note that most significant deviations can be found on the top and bottom plates. That is because of the corrective radial motion of the vacuum chambers applied by the AMD group during installation. The same correction was not possible to be made vertically. An exception are the inner and outer plates of quad Q4 short (Q4S), which have ~ 2 mm average radial deviation from their ideal position. This is a much larger deviation than would be expected to survive after the radial corrective motion of the vacuum chambers. We will revisit and examine further the deviations on the Q4S inner and outer plates in Section 3.2.1. The Q2S inner and outer plates are also out of spec, but not as

Table 2: Average radial and vertical deviations of quadrupole plates from their ideal position. All values in mm.

	Q1S	Q1L	Q2S	Q2L	Q3S	Q3L	Q4S	Q4L
Bottom plate, vertical deviation	2.05	-0.84	-0.49	0.67	1.16	-1.84	-1.16	-0.44
Top plate, vertical deviation	2.42	-1.12	-0.86	0.09	0.34	-2.09	-1.47	0.00
Inner plate, radial deviation	-0.59	-0.53	-0.70	0.06	-0.40	0.31	1.85	0.20
Outer plate, radial deviation	-0.06	0.04	-1.29	-0.13	0.00	-0.08	2.24	-0.03

extremely as Q4S.

02/2018 vacuum incident and repairs On February 2018 a vacuum incident occurred, after which the Q1S and Q4S plates needed to be repaired and reinstalled. Therefore an important caveat to keep in mind is that the Q1S and Q4S locations from the laser scan dataset were only valid up to February 2018. They cannot be directly compared to the in situ surveys that were performed later in 2018, and will be discussed in Section 4.

3.2.1 Large Q4S inner and outer plate displacements

The corrective radial motion of the vacuum chambers was made specifically to null the radial deviations from the ideal position of the inner and outer plates. Therefore the large deviations on these plates in Table 2, which can be ~ 4 times the specified limit, should not exist. If they are real, then the corrective motion must have failed badly.

The laser scan data from Fig. 4 reveal that the Q4S plates were very well aligned relative to the cage, before the cage was installed inside chamber 10. We do not have any data on the alignment of the plates or cage relative to the vacuum chamber. We do however have data of the trolley rails inside the vacuum chambers, obtained from a separate AMD survey using “fiducial” laser reflector markers mounted on the trolley. The data in Fig. 8 are from the reconstructed position at the center of the trolley. The dashed circles in the figure show the final location of the trolley rails if a corrective motion was applied to center radially the position of the Q2S and Q4S inner and outer plates.

The figure makes apparent that the trolley rails would be severely misplaced on the interface of chambers 9-10 and 10-11 if a corrective motion was applied to center the Q4S plates, creating potential problems for the operation of the trolley due to rail discontinuity. Since the rails are fixed relative to the quad plates, the only adjustment possible would be on the adjacent bellows cages. In the past this procedure required several iterations and months before the trolley

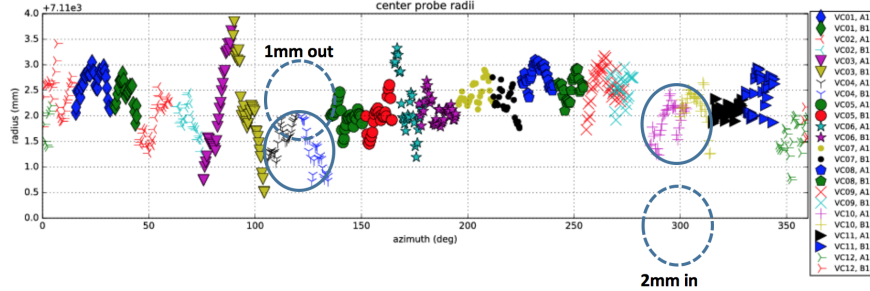


Figure 8: Radial trolley rails position in all vacuum chambers around the ring, from an AMD survey. Ideal position at 2 mm on the vertical axis. The solid circles mark the chambers with radially misaligned quad plates on Q2S and Q4S, chambers 4 and 10 respectively. The dashed circles show the location of the trolley rails after a potential corrective motion to bring the quad plates to their ideal position. Plot edited by Chris Polly based on data from [12].

could operate without getting stuck at a rail discontinuity. A potential move of the chamber would also affect the location of the tracker detectors, the kicker plates, and beam collimators. The latter are especially important, as they have the strictest alignment requirement, ~ 0.3 mm. Any move of the chamber would also require a careful alignment and survey of the final location of all these components.

Finally, the good position of the trolley rails in chamber 10 suggests a potential explanation for the misplaced quad plates: that the corrective motion was performed to center the trolley rails instead of the quads, which would be a mistake. This explanation requires a large misalignment of the trolley rails relative to the Q4S cage, which unfortunately cannot be tested.

Of course the possibility always exists that there may have been an error in the calculation to express the location of the quad plates in storage ring coordinates. The only way to test this is through a survey of the quad plates as installed inside the chambers. For this reason, two independent surveys were performed during the 2018 summer shutdown. They are described in the following section.

4 In situ surveys of quadrupole plates

An effort to survey the EQS plates location in-situ was pursued over the 2018 shutdown. The motivation was three-fold:

1. Firstly, it was important to confirm or disprove the unexpectedly large deviations of the Q4S inner and outer plates deviations. If arising from

a misplacement of their containing vacuum chamber 10, then a corrective action may need to be pursued.

2. After the vacuum incident of February 2018, the position of the reinstalled Q1S and Q4S inner and outer plates was largely unknown, as the laser scan data does not apply anymore. A survey was necessary to get a handle on their location.
3. Lastly, even for the remaining EQS plates where the laser scan data is good, we do not have a good estimation on the uncertainty of that data. For example, it is not easy to quote an uncertainty on the average plate locations quoted in Table 2. Remember that translating the laser scan data to storage ring coordinates rests on the assumption that the plates remained stable and unperturbed when the cage was inserted in the vacuum chamber. That assumption is hard to constrain. Just as the plate location is an important input to systematic corrections to the ω_α analysis, the uncertainty of their location is similarly an important input to the precision of these corrections. Therefore a survey to attempt to constrain that uncertainty is warranted.

Performing in-situ surveys of the quad plates is quite challenging, mainly due to the difficulty of access to the plates from inside the storage region. It is certainly impossible for the laser scanning system to sample from inside the storage region due to its bulk. Many other options considered have similarly forbidding high volume, either in the sensors or the accompanying cables and readout electronics. For example the Capacitec sensors were initially considered, but the bulky readout electronics would have to remain outside the chamber and connected to the sensors over long cables, which would have to be carefully unspooled and collected through flanges as the trolley moves. Other than very cumbersome, it is strongly preferred that such long cables are avoided since they could get caught on the plates, rails, or other components, and cause damage. Besides there were concerns with the reliability of measurements from the Capacitec probe. Any sensor that could be used inside the storage region must also have an operational range that matches the geometry, and achieve sub-mm precision to give a meaningful comparison to the existing data.



Figure 9: The Keyence sensor head emits a laser beam and estimates distance from an object by detecting its reflection.

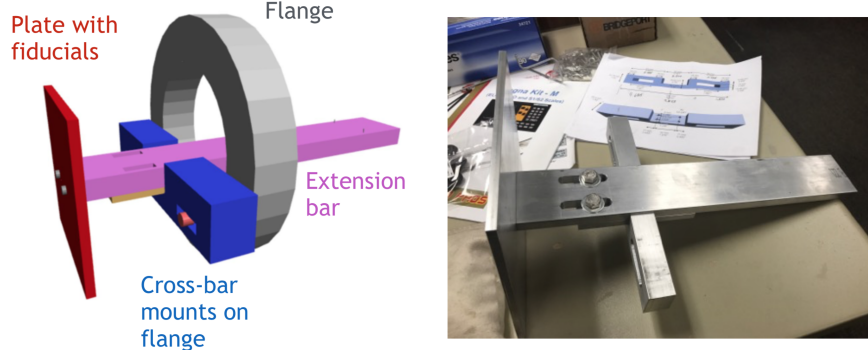


Figure 10: Left: The design for the fixture that will mount on a flange and hold the Keyence sensor. Right: The fixture after machining and assembly.

An alternative is to sample externally through the flanges. This option however provides access only to the inner plate, and only to its face that is outside the storage region. The access through flanges is also extremely limited azimuthally. Finally, any distance measurement should be performed without any contact to the plates, or at least with very careful and slight contact, as to avoid bending and modifying the plates.

Two completely independent in-situ measurements were developed and performed during the 2018 shutdown, overcoming the challenging limitations. They are described in this section.

4.1 Through-flange extension probe

The first measurement aims to use a high-precision sensor to estimate the uncertainty of the laser scan data. Working together with the AMD group, we selected the Keyence LC-2220 optical displacement sensor for our measurement. The Keyence system utilizes a 670 nm wavelength semiconductor laser to achieve μm -level resolution. The sensor head is shown in Fig. 9.

The sensor is connected through a cable to a bulky laser head, control and readout unit, so it was not feasible to measure from inside the storage region. This probe is meant to survey the EQS plates through flanges. The disadvantage of this choice, as mentioned above, is that we only get access to the inner side of the inner plate and only over a small azimuthal range. An advantage is that the measurement can be translated to storage ring coordinates by correlating each surveyed location to laser finder markers placed in known positions around the ring.

Another consideration is that the Keyence sensor has a small linear operating range of 3 mm and has to be placed 30 mm away from the object. A fixture was designed to mount on a flange, with an extension bar to bring the Keyence sensor to about 30 mm from the inner quad plate. The fixture is shown in Fig. 10. The extension was designed to be adjustable to allow for variations, but the AMD

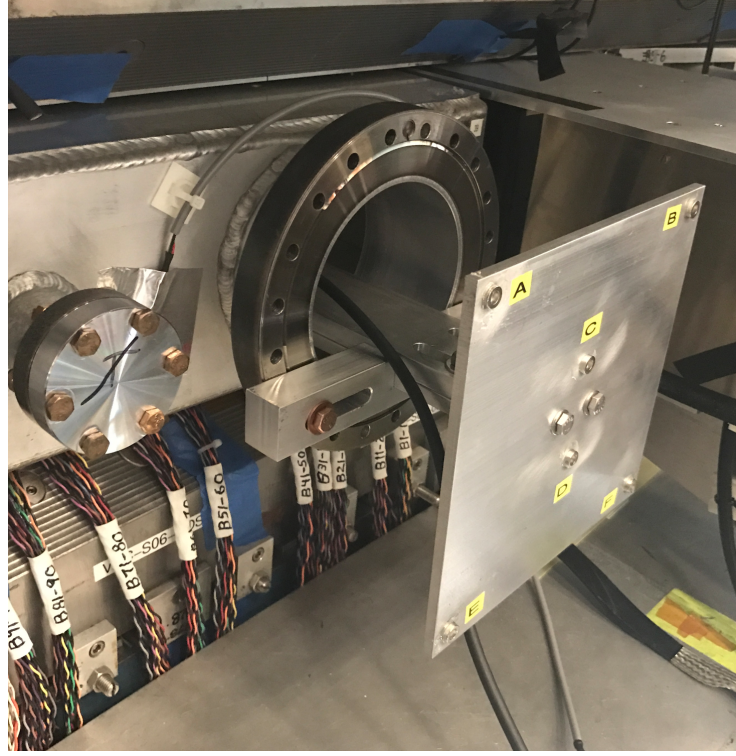


Figure 11: The fixture mounted on a flange, with the Keyence sensor head (unseen) at the edge of the extension bar sampling a quadrupole plate, connected through a cable to the laser head. Fiducial markers are fixed on the back-plate, each identified by a letter.

group decided to keep the extension length fixed to simplify calibration of the probe. This choice however meant that the distance between the flange and the plate had to be constant, which allowed us to use only one flange per quad plate (with design distance of 31 cm between the flange and the quad plate), narrowing the azimuthal coverage even further. To partially make up for that, the mounting of the fixture onto the flange was also adjustable to allow multiple measurement points per flange. Finally on the back of the fixture a plate was installed where the fiducial markers will be fitted.

The Keyence sensor was calibrated using a precision translation stage and calipers to confirm the real distance from the object. The sensor's reading versus the actual distance is shown in Fig. 12. The reading is shown to be very repeatable over multiple passes, after powercycling, and with multiple objects. However, outside the linear operating range of 30 ± 3 mm, the reading initially switches to "NEAR" or "FAR", but upon going out further we get back a reading of distance again. We suspect that this reading may arise from reflections inside

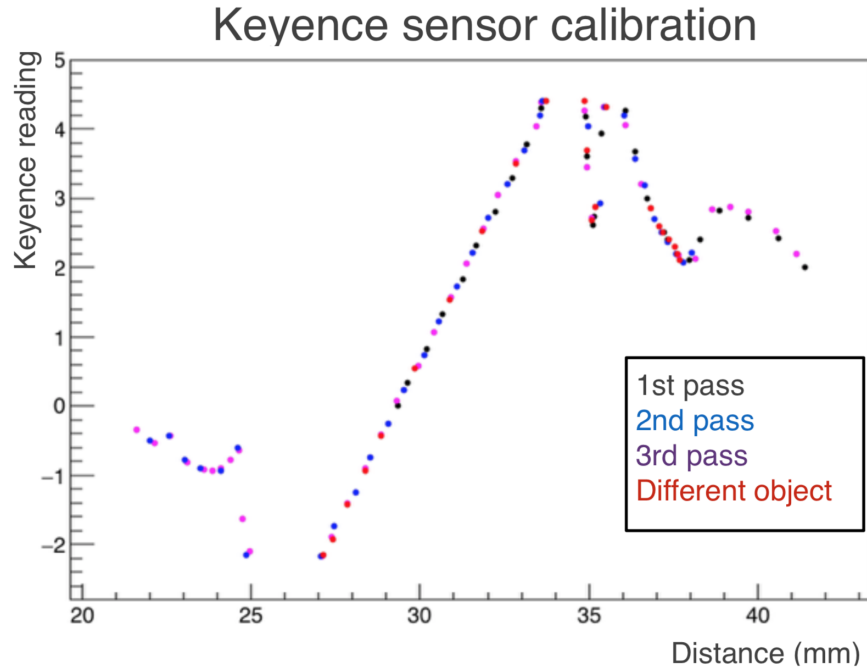


Figure 12: Calibration of the Keyence sensor. The sensor is very repeatable, but has a limited linear range.

the sensor head. This is concerning, as in principle we are not able to distinguish whether a reading of *e.g.* -0.8 mm is from the linear region or arising from reflections, without further information.

A first attempt to survey the plates with the Keyence sensor gave some confusing results, partly due to the uncertainty in the sensor's calibration [13]. It was desirable that an independent measurement with a different probe could be mounted on the same fixture, preferably measuring concurrently, to remove any ambiguity from the Keyence sensor. The confirmation probe does not need to have the same high precision as Keyence. To that end, a manually controlled extension rod that samples the plate by contact, was installed and could be operated concurrently with Keyence. The contact should be as soft as possible to avoid any impact on the plate's position. The precision achieved should be better than 1 mm , good enough to confirm the Keyence measurement with completely independent systematics.

4.1.1 Extension probe dataset

The fixture with the Keyence sensor and the extension rod was used to sample 6 out of the 8 quadrupole plates on 12/13/2018[14]. The remaining 2 plates were

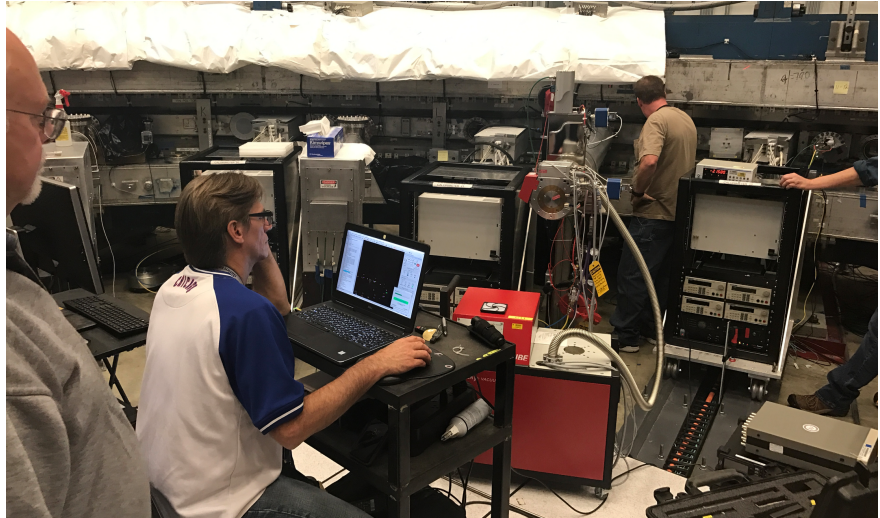


Figure 13: The AMD group is fitting the location of the fixture with a laser finder system. Meanwhile the Keyence sensor, with its head mounted on the fixture's extension, reads a distance of 2.1580 mm from the quad plate.

not sampled as the required flange was occupied on their containing chamber. One of the plates not sampled on that day was Q4S, but we have data on that plate from a previous iteration of the measurement only with the Keyence probe.

A group from AMD came to correlate the position of the fixture to known fiducial markers around the ring. The fixture holding the two probes is mounted on the lone open flange, respecting the requirement that only one flange can be open at a time to prevent significant vacuum contamination. The Keyence sensor samples the inner face of the inner quad plate and gives a distance reading. Then a person from the AMD group softly pushes on the extension rod until contact is made with the plate. We can see the Keyence distance reading increase by ~ 0.2 mm with the rod pushing on the plate. The operator then slightly pulls back the rod. Unfortunately, we found afterwards that the operator pulled until the Keyence reading returned to the original value, although a small offset should have been allowed to verify contact.

Based on pre-calibration on the rod, we can immediately confirm that the Keyence sensor is within its linear range of operation. With both probes in place, the laser finder system locates the fiducial markers on the back of the fixture. We repeat the procedure by repositioning the fixture on the flange for one more measurement, and then move on to another flange.

All results are listed in Table 3. There were two measurement locations per quad half-segment, *i.e.* two different mounts of the fixture on the flange, marked as *a* and *b* in the table. The variation in [Theta,Z] location is usually very small between these two measurements, and so is the extracted R. But it is still good practice to sample at least twice on each plate. For each of the two locations,

Table 3: Survey data from the Keyence and extension rod probes, and comparison to the laser scan data.

	R (mm)	Theta	Z (mm)	Diff. Rod- Keyence	Diff. to laser scan	Avg diff per plate
Keyence, Q1Sa	7061.804	-40.231	17.524		0.816	
Rod, Q1Sa	7061.580	-40.358	11.757	0.2	0.470	
Keyence, Q1Sb	7061.882	-40.134	17.528		0.912	
Rod, Q1Sb	7061.743	-40.260	11.784	0.1	0.627	0.706
Keyence, Q1La	7061.903	-70.167	16.591		0.632	
Rod, Q1La	7061.730	-70.295	10.674	0.2	0.531	
Keyence, Q1Lb	7061.664	-70.224	16.706		0.382	
Rod, Q1Lb	7061.459	-70.351	10.888	0.2	0.174	0.430
Keyence, Q2Sa	7061.764	-130.236	2.828		0.569	
Rod, Q2Sa	7061.257	-130.365	-3.206	0.5	0.251	
Keyence, Q2Sb	7061.703	-130.104	2.737		0.585	
Rod, Q2Sb	7061.287	-130.233	-3.275	0.4	0.403	0.452
Keyence, Q2La	7062.036	-160.230	17.338		-0.128	
Rod, Q2La	7061.790	-160.359	11.411	0.2	-0.411	
Keyence, Q2Lb	7062.054	-160.127	17.009		-0.118	
Rod, Q2Lb	7061.743	-160.255	11.220	0.3	-0.461	-0.280

(cont'd)

(cont'd)

	R (mm)	Theta	Z (mm)	Diff. Rod- Keyence	Diff. to laser scan	Avg diff per plate
Keyence, Q3La	7061.238	109.891	16.856		0.364	
Rod, Q3La	7061.000	109.762	11.017	0.2	-0.129	
Keyence, Q3Lb	7061.093	109.794	16.959		0.221	
Rod, Q3Lb	7060.971	109.666	11.172	0.1	-0.171	0.072
Keyence, Q4Sa	7061.043	49.735	-4.003		2.777	
Keyence, Q4Sb	7061.100	49.920	-4.109		2.780	2.778
Keyence, Q4La	7063.608	19.885	16.658		-0.149	
Rod, Q4La	7062.723	19.758	10.887	0.9	-1.048	
Keyence, Q4Lb	7063.644	19.825	16.685		-0.056	
Rod, Q4Lb	7063.587	19.698	10.964	0.1	-0.202	-0.364

both Keyence and the extension rod give a measurement of the radial location of the plate. This is expressed as the radial location of the muon-side surface of the inner plate, under the assumption of a constant ideal plate thickness. The points sampled by the two probes are generally separated by approximately 0.13° azimuthally and 6 mm vertically.

Looking at the difference between the Keyence sensor and the contact rod, it is good to observe that it is generally smaller than 0.5 mm. That is a good confirmation that both independent measurements are reliable, given also that a small variation might be expected from the small offset in the points surveyed from the two probes. However, the difference between them is always positive, meaning that Keyence always gives a higher radial location than the rod on the same measurement. This is very likely a systematic error on the result from the contact rod based on the measurement procedure described previously, which means that the rod may not make perfect contact with the plate. This is also likely the reason for the biggest discrepancy of 0.9 mm between the two probes on measurement VC11a. Given the method of manually pulling back, such a large systematic error could be possible. Notice also that the rod measurement Q4Lb is in good agreement with Keyence on that location, even though variation between the two measurements on the same flange from the same probe is gen-

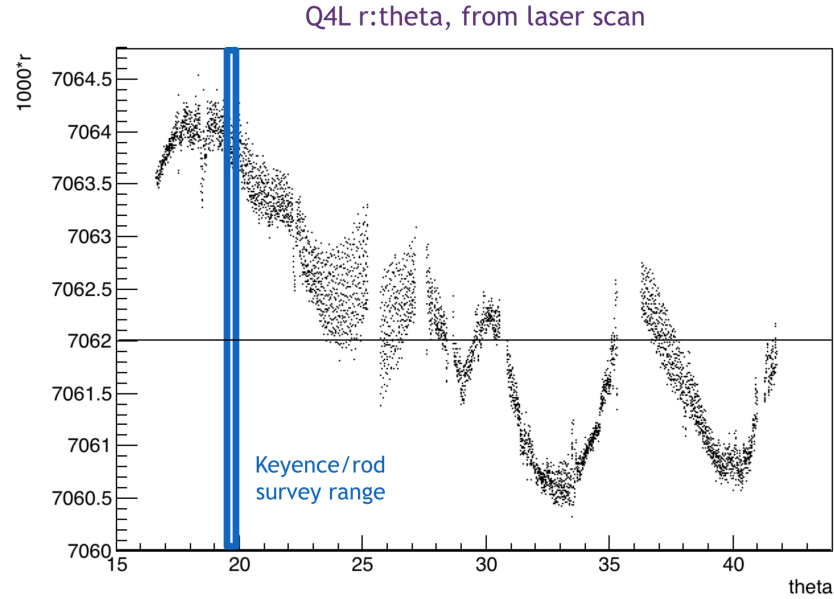


Figure 14: Radial position versus azimuth for the Q4L inner plate from the laser scan data. The azimuthal range sampled by the probes through a flange is contained within the blue box.

erally within 0.2 mm. Therefore we have a reasonable and probable explanation for that largest discrepancy.

On the difference to the laser scan data, the results on plate Q4S stand out immediately due to the high discrepancy of ~ 2.8 mm. As noted earlier the measurements on that plate were performed before the extension rod was also mounted on the fixture. It is clear however that the in situ survey does not support the large misalignment suggested by the laser scan. If anything the radius is found to be smaller than ideal, but it is hard to make that statement having only sampled a small azimuthal range. Given that such a large offset would be difficult to explain from modifications during re-installation of the plate, the leading explanation currently is that there may have been a calculation error in the estimation from the laser scan dataset.

On all other plates, it is very good to observe that all individual measurements from both probes have a difference smaller than 1 mm from the laser scan expectation, calculated around the same (θ, z) coordinates. The one exception is the rod measurement Q4La, but we have already established that this is probably due to the rod not being in good contact with the plate. In fact the sign of the discrepancy is consistent with that explanation, and all other measurements on that plate are in very good agreement. The differences are larger on the Q1S plate, but this is the reinstalled plate so we do not expect the laser scan data to be valid there anymore.

Finally on the last column we give the average difference between the direct in-situ surveys and the laser scan expectation. With the exception of the Q1S plate where the comparison is not meaningful, the average difference per plate is always smaller than 0.5 mm. That is very good agreement, and a very good indication for the size of uncertainty in the laser scan dataset.

It may be noted that the radial position sampled on Q4L is rather far from the design 7062 mm, almost by 2 mm, while the average radial deviation from Table 2 was only 0.2 mm on that plate. The explanation for this is shown in Fig. 14. Within the range sampled by the in-situ surveys the deviation from ideal happens to be large, even though the average is in good agreement. This figure also illustrates the small azimuthal range of the plate sampled by the Keyence and extension rod. The in-situ survey discussed in the following section covers the entire azimuthal range of each plate, and is therefore very valuable.

4.2 Proximity sensors mounted on the trolley

An alternative ambitious idea to sample the quad plates from inside the storage region, using proximity sensors mounted on the field trolley, is presented in this section. The main motivation for this was to get enough data to extract an average location for the unknown Q1S and Q4S plates. This would be impossible to get with just a measurement through flanges due to the limited azimuthal coverage and the potential for significant azimuthal variation on the plate location. But the hope was that this measurement could achieve good enough precision to be meaningful in the estimation of the laser scan data uncertainty.

The proximity sensors selected based on these requirements are the VCNL4010 from Vishay Semiconductors [15].

The VCNL4010 proximity sensor is a fully integrated infrared emitter and PIN photodiode at a matched wavelength, with 16-bit ADC resolution. The chip also includes an ambient light sensor which was not used. The proximity measurement is nicely independent of ambient light by modulating the infrared signal.

The chip is controlled via I²C interface from a Raspberry Pi (Rpi) board. Because we need to operate two VCNL4010 chips concurrently, and since the chips have the same immutable slave address, the second I²C bus of the Rpi was activated and the two chips

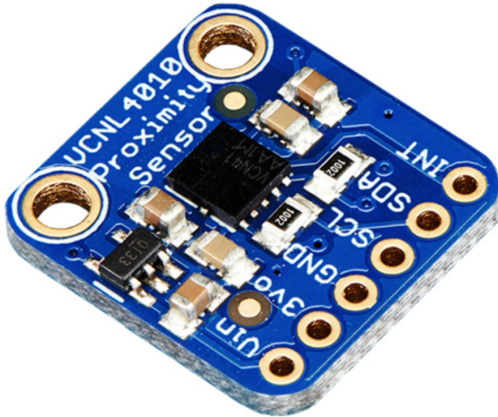


Figure 15: The VCNL4010 proximity sensor chip.

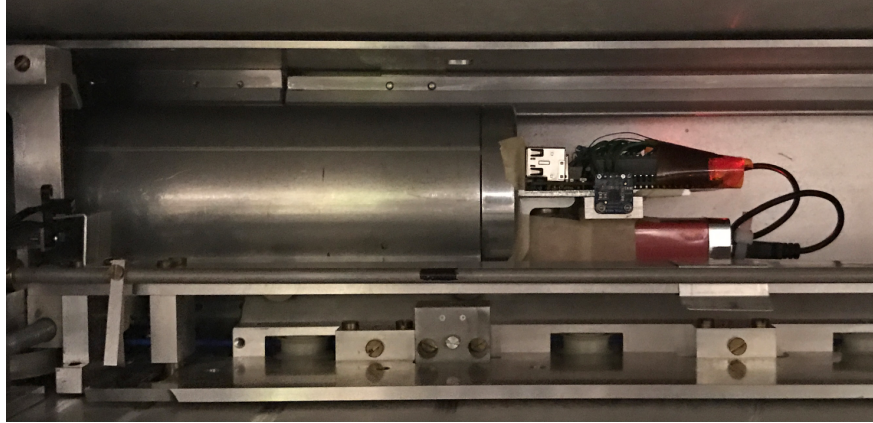


Figure 16: The fixture with the Raspberry Pi, proximity sensors, and battery, mounted on the trolley, as seen through the trolley garage.

were controlled over separate buses. The 5 V input to the Rpi can be provided by a 4000 mAh battery with a lifetime of a few hours, so the entire measurement can be made autonomous and independent of cables and any device outside the chambers.

An important requirement is that the sensors must be able to perform the measurement from at least 5 mm from the object, as there are locations in the ring where the radial clearance is more snug than inside the quad plates, which are 100 mm radially apart. One such region is at the kicker plates, which have only \sim 94 mm radial clearance. Another is at the inflector entrance, which probably allows the smallest clearance on the outer side relative to the center of the storage region, about 46 mm. Therefore the sensors must be able to measure from a distance, in order to be mounted on the trolley and safely pass through these snug regions. The trolley itself has a 90 mm diameter and it has often been difficult to operate without interference with the kicker plates.

Based on this a fixture was designed to bring them close enough to the plates for a precision measurement. Two VCNL4010 sensors were placed opposite each other to sample the inner and outer plates concurrently. They were mounted on a bar with a radial extent designed to place the sensors on a distance from the quad plates which balances precision and safety. The fixture must be mounted on the vertical surface of the trolley, which is circular with 90 mm diameter, using nothing but tape. Tests were performed to ensure that the fixture can be mounted safely, as a fall of the fixture inside the vacuum chambers could be dangerous. Furthermore, the fixture could only be mounted through the trolley garage after the trolley was already on its rails. Mounting sideways and from a significant distance made centering of the fixture onto the trolley's vertical surface quite challenging at the mm-level.

4.2.1 Scraping of sensors in vacuum region

On a first iteration of the VCNL4010 measurement from the trolley, upon retrieving the fixture it was discovered that the sensor sampling the outer plates had scraped somewhere inside the vacuum region and had dropped 3 small surface mount components (Fig. 17).

The interaction was not immediately detected, as the Rpi could not be read-out while inside the vacuum chamber. Wireless ssh connection with the Rpi was forbidden by the Fermilab network, and an attempt to upload the data to a remote repository failed as wireless connection inside the chambers was unreliable. It was thought that any interaction of the sensors would induce enough tension on the trolley pulling cables to trip the trolley motion, but this was not the case. The reason for the interaction in the first place was that the difficulty of centering the fixture on the trolley surface was underestimated, resulting in significant placement offset towards larger radii. As we will see in Appendix A we were unlucky in the direction of this offset, as the kickers are misaligned inwards by up to a few mm.

We should have been much better prepared and made sure that all precautions were in place to avoid any such interaction in the vacuum region. In the following section we list the lessons learned and all the improvements that were made to repeat the measurement successfully.

The biggest concern with the dropped components was a potential perturbation to the magnetic field inside the storage region, as they were all ferromagnetic. Even if small, it was concerning that the perturbation would probably be different every time the magnet cycles and the components move. Fortunately we were able to predict that the interaction probably occurred near the downstream end of kicker plates K3, through an analysis of the VCNL4010 sensors data before the interaction [16], and through a comparison of the trolley cables tension to baseline runs without the sensors [17].

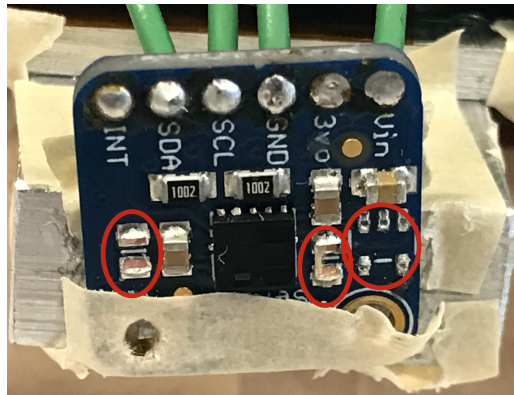


Figure 17: The VCNL4010 chip after interaction. Surface mount components scraped and dropped inside the vacuum chambers.

4.2.2 The VCNL4010 dataset

Several lessons were learned from the incident of the sensors scraping inside the vacuum region, and improvements were made in the measurement design to

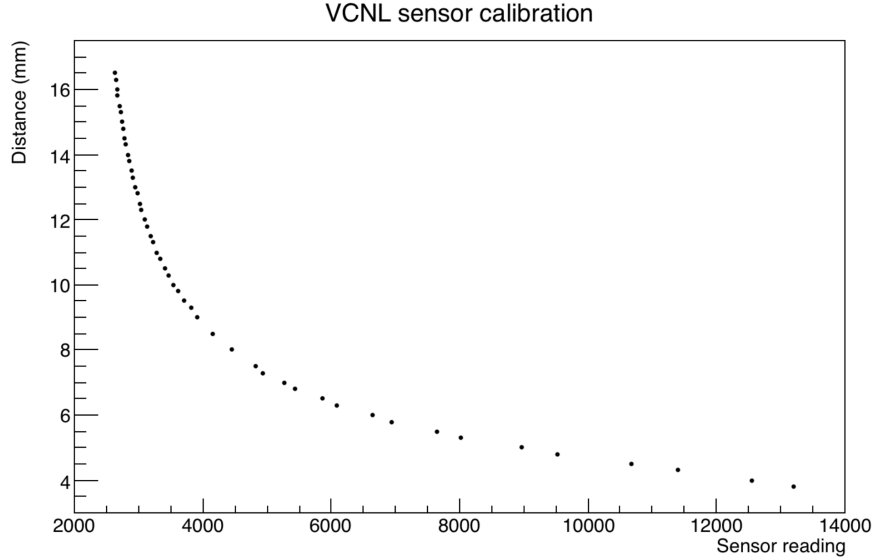


Figure 18: Calibration for one of the VCNL4010 sensors. The dataset contains two separate measurements to ensure reproducibility. The sensor reading changes more rapidly at a distance of 7 mm compared to 10 mm, so increasing the distance between the sensors and the sampled plates for safety reasons came with a loss in resolution.

prevent similar failures from happening again.

1. **Radial extent of sensors.** Based on the sensors' calibration (shown in Fig. 18) they could be placed a few mm further from the quad plates and still achieve adequate precision. Therefore the radial extent of the bar was reduced from 80 down to ~ 74 mm, designed to place each sensor ~ 10 mm from the quad plates (the sensors also have 3 mm thickness) and increasing the allowance for an offset of the fixture's placement.
2. **Centering of fixture on trolley surface.** An alignment system was devised for mounting of the fixture, which should have prevented the interaction in the first place. The scheme adds another part to the fixture and uses tape to provide guidance when mounting from the side. A better yet centering mechanism was considered but machining resources were very limited to pursue in time. Should this measurement be performed again in the future, this more robust centering scheme will be constructed.
3. **Readout** was a significant vulnerability. Without readout we are blind to the true location of the sensors after mounting and can only guess the potential placement offset. We resolved to connect with the Rpi through ssh over an ethernet cable (this got the Rpi blocked from the Fermilab network) after it was mounted on the trolley. Then the trolley moves

upstream by a few azimuthal degrees as we carefully hold the ethernet cable, until the sensors sample the Q2L plates to roughly confirm good placement of the fixture. Then we bring the trolley back to the garage, remove the ethernet cable, and begin the run around the ring.

After the fixture modification and following the procedure outlined above to confirm good placement, on 12/12/2018 the trolley ran through all EQS plates around the ring allowing the two VCNL4010 sensors to sample the inner and outer plates continuously. The collected data versus run time is shown in Fig. 20, where the vertical axis is the measured distance from the sensors to the plates. The distance was extracted from the sensor's raw ADC reading based on the calibration from Fig. 18.

To translate the VCNL4010 proximity measurement to position of the plates in storage ring coordinates, we don't have the convenience of the AMD laser finding system for each measurement. Instead the baseline plan is to use the "known" EQS plates. By matching the data on those plates, we can then go on and have a reliable estimation of the location of the unknown plates Q1S and Q4S.

A more ambitious approach is to use the location of the trolley rails, which is known from an AMD survey (as in Fig. 8). From that AMD survey we use specifically the location of the fiducial marker positioned on the downstream face of the trolley, the same where the VCNL fixture was mounted and therefore most relevant. An example of the trolley location around Q1S is shown in Fig. 21. We preferred to fit the data for each quad so that the radial center of the trolley rails can be extracted for each azimuthal position. For details on this procedure see [18].

We need one more piece to express the proximity measurement as a radial plate location, and that is the distance from the center of the rails to each sensor. Unfortunately this cannot be known independently with precision better than 2 mm, as it was not possible to make that measurement before dismounting the fixture from the trolley. Furthermore, this unknown factor may also pick up contributions from a potential rotation and/or vertical misplacement of the fixture, complicating its definition.

We determine these geometric factors by matching the sensor data to the known plates' location from the AMD laser scan. Specifically the values for these factors are chosen to minimize the difference (between the sensors and the laser scan data) in the average radial position of the inner and outer plates of the known quads, *i.e.* excluding the reinstalled Q1S and Q4S. The mylar plate Q1L outer was also excluded from this calculation, as the comparison between VCNL4010 and the laser scan was most inconsistent there, as we will see in Table 4. This may be due to the sensors not sampling the wavy mylar accurately, or perhaps the mylar plate was most modified relative to the laser scan when its cage was inserted to the chamber. Either way we are justified to exclude this plate.

We can now get the result for the position of the quads plates by combining:

- the trolley rails location from the AMD scan,

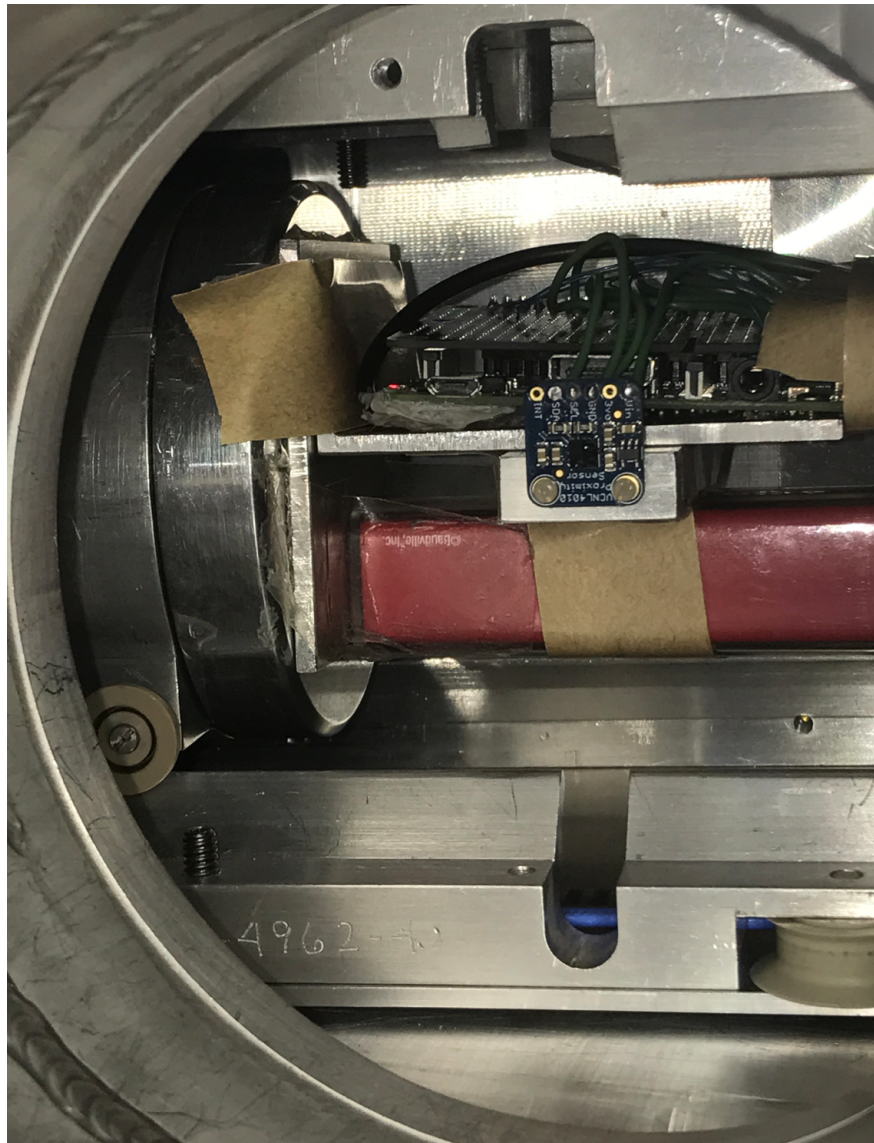


Figure 19: The fixture mounted on the trolley as viewed through a flange. Visible is the VCNL4010 sensor that samples the inner quad plates, the Raspberry Pi board, and the battery in red.

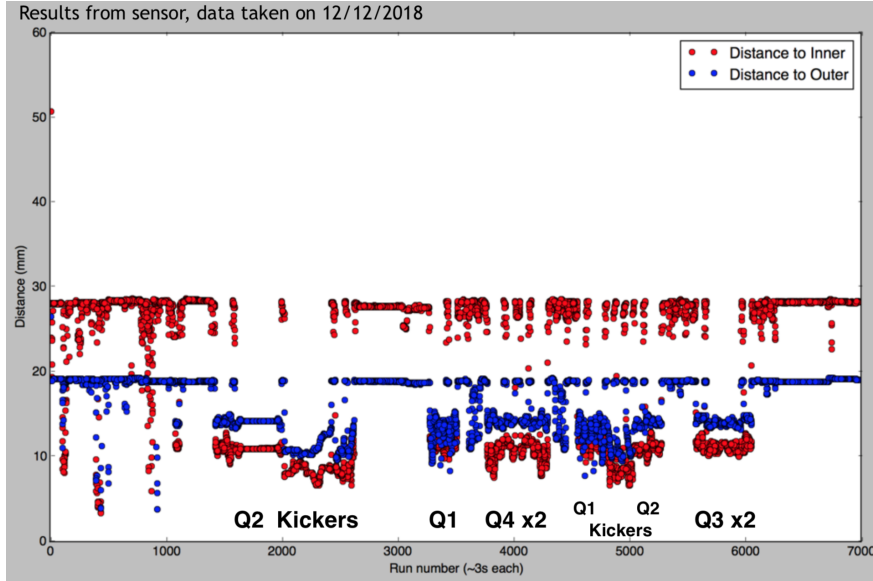


Figure 20: The raw data collected by the VCNL4010 sensors facing opposite plates, plotted versus run time. Locations of quad and kicker plates are indicated.

- the parameter for the distance from the center of the rails to each sensor, extracted from fitting to the laser scan data, and
- the proximity measurement of the sensor based on its calibration.

The collected data versus time from Fig. 20 can be mapped onto azimuthal location since it is obvious where each plate starts and ends, and given that the trolley is moving with mostly constant velocity.

As an example we plot the VCNL4010 results for the position of the inner and outer plates of Q3L in Fig. 22. The VCNL results are the red triangles. There are actually two kinds of triangles, pointing up or down, for the two opposite directions in which the trolley passed through Q3L. The agreement between the two measurements is excellent, giving confidence to the reliability and reproducibility of the sensors.

Also plotted in black are the laser scan data. Highlighted in green are the laser scan data from within 5 mm from the vertical center, which should correspond roughly to the area sampled by the VCNL sensors. The agreement between the two independent surveys is very good, especially in reproducing the radial variations across the length of the inner plate.

Finally on the same plot are the results of the survey performed through a flange, as described in Section 4.1, plotted as blue crosses. Of course these only exist for the inner plate, which was the only one sampled. Again we notice the very limited azimuthal coverage. The large RMS of the laser scan data around

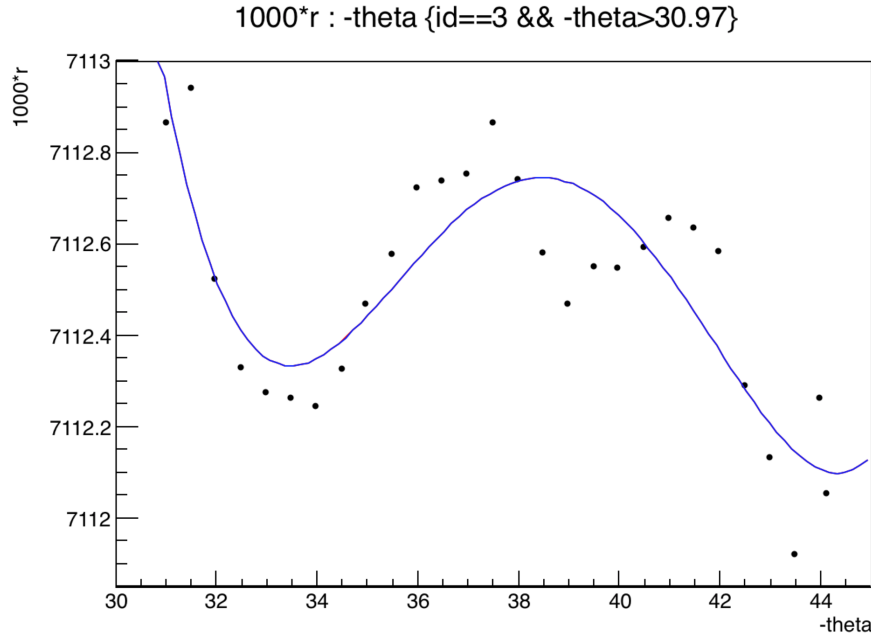


Figure 21: Location of trolley rails through Q1S from an AMD scan (black points, for the downstream marker only). The data is fitted with a function (blue line) which can be used in any azimuthal location. Residuals are generally within 0.1 mm.

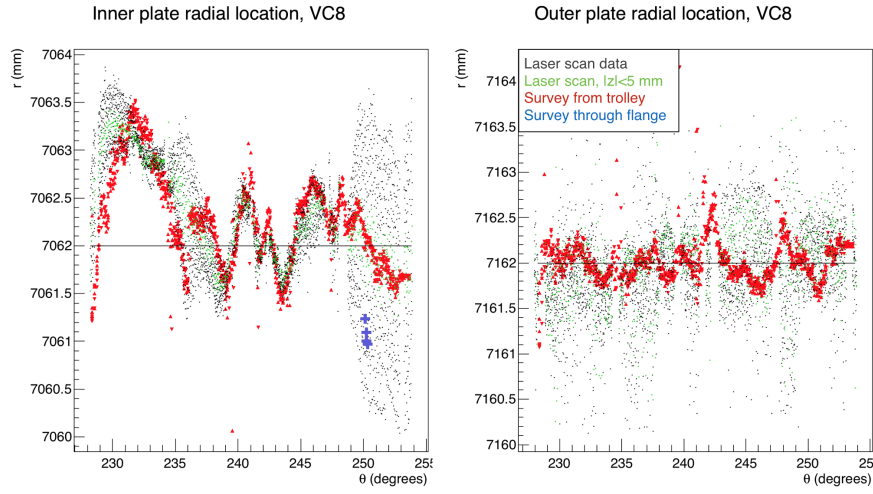


Figure 22: Surveys of the Q3L inner and outer plates in vacuum chamber 8. See text for details.

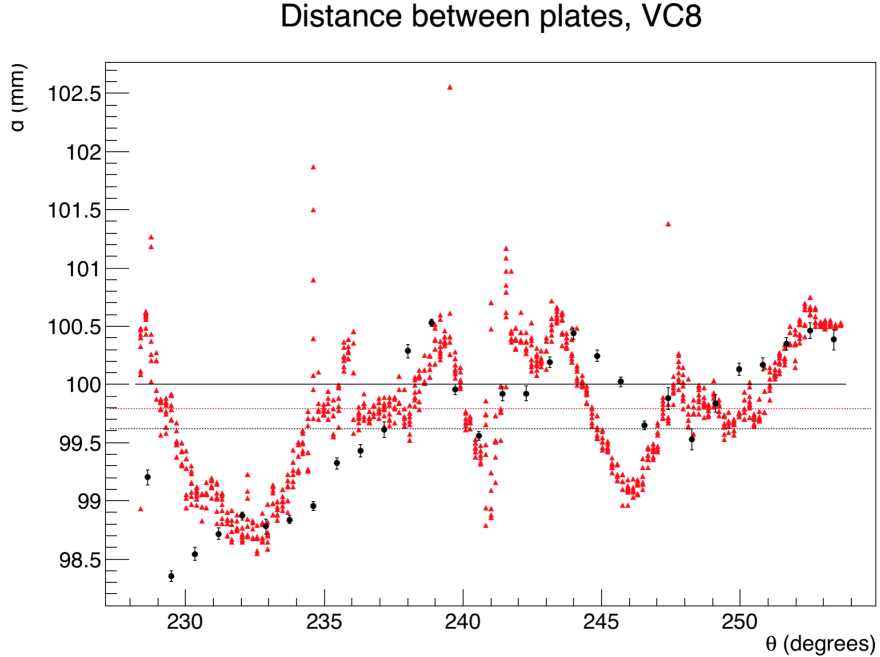


Figure 23: Distance between inner and outer plates of Q3L, from the VCNL4010 sensors (in red) and from the laser scan (in black).

$\theta = 250^\circ$ suggests a significant tilt of the plate around the region sampled by the probes on the extension fixture. Since we don't have any information on the vertical coordinate in this figure (other than the green points which are taken around the vertical center) comparison of these survey results is not straightforward, but from Table 3 we see that the agreement with the laser scan is quite good.

Another quantity of interest is the distance between the opposite inner and outer plates, which is important for the actual electric field felt by the muons inside the storage volume. This distance as extracted from the VCNL sensors and from the laser scan is plotted in Fig. 23 for Q3L. The average distance over the entire plate is shown as a dashed line of the corresponding color for each survey. Again the agreement is good, less than 0.2 mm between the two surveys. The design value of 100 mm is shown as a solid line. Both surveys agree that the average distance between the plates is slightly smaller than designed, which will lead to slightly stronger defocusing in the horizontal plane on Q3L.

The data from all surveys and for all plates can be found in [19].

In Fig. 24 we show the survey results on the inner and outer plates of Q4S. It is clear that there is a large discrepancy between the laser scan data and the in situ surveys. The VCNL data are consistent with the design position of the Q4S plates, and also the agreement between the two independent in situ surveys is

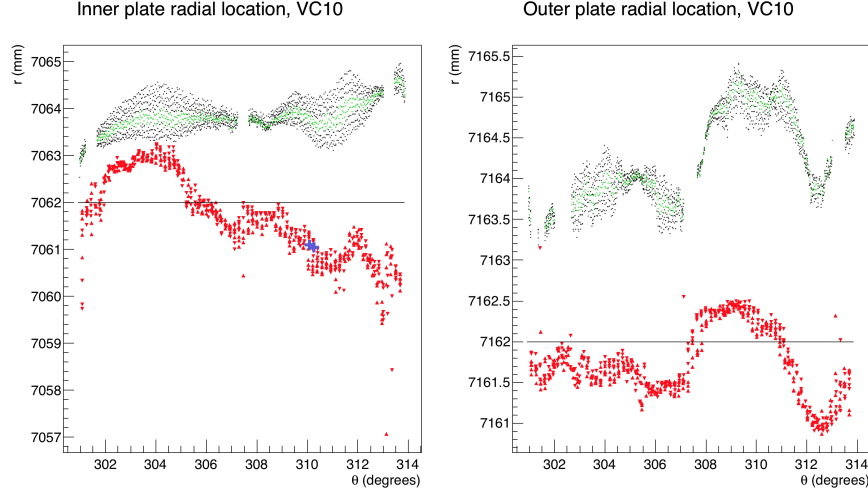


Figure 24: Surveys of the Q4S inner and outer plates in vacuum chamber 10.

excellent. This supports the hypothesis that there could be a calculation error on the laser scan result. We notice also that the VCNL survey reproduces the azimuthal dependence of the radial position of the outer plate but not of the inner, suggesting that perhaps only the latter was modified upon reinstallation. In any case, the in situ surveys conclusively exclude the need for a potential corrective motion on the chamber.

The average radial position of each quad inner and outer plate is listed in Table 4, from each survey. It can be seen that the difference between the VCNL survey and the laser scan is always within 0.5 mm, with the exception of the mylar Q1L outer plate. It is clear then that the ± 2 mm discrepancy on the Q4S plates is likely due to an error in the laser scan calculation.

The average difference in the radial position from the laser scan and the VCNL survey is listed in Table 5. The difference is averaged over all plates where the comparison is valid, *i.e.* excluding the reinstalled Q1S and Q4S, as well as the mylar Q1L outer. We call these the "known" quads: Q1L (excluding here the outer mylar plate), Q2S, Q2L, Q3S, Q3L, Q4L. It is not surprising that the average difference is very small. Remember that we fixed the VCNL geometric factors exactly to minimize this difference over the quads where we know the laser scan data to be good. The important point here is that the RMS of this difference over each plate is also very small. This suggests that the average difference would be well constrained even if we had picked a random quad to fix the VCNL parameters.

Table 4: Average radial position of quadrupole plates, comparison between different surveys. All values in mm.

		Laser scan	VCNL	Difference Scan-VCNL	Difference Scan-Extension
Q1S	Inner	7061.41	7061.58	-0.16	0.706
	Outer	7161.94	7161.44	0.51	
Q1L	Inner	7061.47	7061.30	0.18	0.430
	Outer	7162.04	7160.63	1.41	
Q2S	Inner	7061.30	7061.31	-0.01	0.452
	Outer	7160.71	7160.76	-0.05	
Q2L	Inner	7062.06	7061.77	0.29	-0.280
	Outer	7161.87	7161.77	0.11	
Q3S	Inner	7061.60	7061.51	0.08	0.072
	Outer	7162.00	7162.41	-0.41	
Q3L	Inner	7062.31	7062.23	0.08	0.072
	Outer	7161.92	7161.79	0.13	
Q4S	Inner	7063.85	7061.61	2.24	2.778
	Outer	7164.24	7161.70	2.54	
Q4L	Inner	7062.20	7062.64	-0.44	-0.364
	Outer	7161.97	7161.58	0.39	

Table 5: Difference between the radial positions from the laser scan and from the VCNL survey, averaged over all the plates where the comparison is good. All values in mm.

	$\langle \Delta r \rangle$	RMS
”Known” inner plates	0.03	0.23
”Known” outer plates	0.03	0.26

5 Location and uncertainty of quadrupole plates

Combining our knowledge from the three different surveys, which are overall in very good agreement, we arrive at our best estimation for the location of EQS plates and estimate the uncertainty.

For the ”known” quads, apart from Q1S and Q4S which were reinstalled, the laser scan data are the best estimation and define their location. The uncertainty can be extracted from the high-precision measurement with the extension through the flange. From the *Diff. to laser scan* column in Table 3, that difference averages less than 0.5 mm per plate. We will use that conservatively as the baseline for each plate’s location uncertainty. We may increase that baseline uncertainty for the outer plates, which were not sampled. We use 0.7 mm, which is the largest entry in that column, even if in comparison to Q1S laser scan data

Table 6: Radial position and uncertainty contributions for each quad plate. All values in mm.

	Avg r	Difference Scan-Extens.	Difference Scan-VCNL	Unknown plates	Total uncertainty
Q1S	Inner 7061.58	0.7	0.5	0.5	0.99
	Outer 7161.44	0.7	0.5	0.5	0.99
Q1L	Inner 7061.47	0.5	0.18		0.53
	Outer 7162.04	0.7	0.44		0.83
Q2S	Inner 7061.30	0.5	0.01		0.50
	Outer 7160.71	0.7	0.05		0.70
Q2L	Inner 7062.06	0.5	0.29		0.58
	Outer 7161.87	0.7	0.11		0.71
Q3S	Inner 7061.60	0.5	0.08		0.51
	Outer 7162.00	0.7	0.41		0.81
Q3L	Inner 7062.31	0.5	0.08		0.51
	Outer 7161.92	0.7	0.13		0.71
Q4S	Inner 7061.61	0.7	0.5	0.5	0.99
	Outer 7161.70	0.7	0.5	0.5	0.99
Q4L	Inner 7062.20	0.5	0.44		0.67
	Outer 7161.97	0.7	0.39		0.80

before the vacuum incident.

Since the extension survey only covers a small azimuthal range, we will add in quadrature as uncertainty the average radial difference from the VCNL survey, which is listed in the *Difference Scan-VCNL* column in Table 4. But we will not use that metric on the mylar plate Q1L outer, where we cannot fully trust the VCNL sensors. In fact the discrepancy between the laser scan and the VCNL sensors is localized on the larger "waves" of the mylar (see pg.5 of [19]). Previous analysis [20] has shown that plate waviness has small effect on beam dynamics, as would be expected for small-scale ("high-frequency") structure, and therefore is not correct to assign as uncertainty for the average radial location. For that plate we assign 0.44 mm uncertainty term, the largest entry for a known quad in that column.

For Q1S and Q4S which were reinstalled after the vacuum incident, our best estimation for their location comes from the VCNL survey. On Q1S the difference is not significant anyway, but on Q4S we finally remove the 2 mm discrepancy that probably comes from a calculation error. The baseline uncertainty of the average radial location will be 0.7 mm, the largest discrepancy between the laser scan and extension probes which is found on Q1S. Of course

the comparison is not applicable on Q1S as the laser scan data is no longer valid, but that is also why a largest uncertainty is justified.

Since the best information on the Q1S and Q4S plates comes from the VCNL survey, we also need to add uncertainty for the discrepancy between that survey and the laser scan dataset. We will use 0.5 mm, the largest deviation on an individual plate (found on Q1S outer, excluding the miscalculated Q4S plates and the Q1L outer mylar plate) from the *Difference Scan-VCNL* column in Table 4. We also assign uncertainty based on the procedure to fix the geometric factors needed to express the VCNL survey into storage ring coordinates. We essentially calibrated the survey results on the known plates, in order to extend them to the unknown ones. The small RMS from Table 5 is a good measure of the stability of this process. We conservatively use twice that RMS, 0.5 mm, as uncertainty for extending the survey to the unknown plates.

The final results for quad plate position and associated uncertainty are quoted in Table 6.

6 Conclusion

A significant effort was invested over years and by several people towards a precise determination of the EQS plates alignment. The rich laser scan dataset, corroborated and amended by the *in situ* surveys performed over the 2018 shutdown, combine into our best estimation for the plate positions listed in Table 6. Comparison between the independent surveys yields also an estimation of the uncertainty of each plate’s location, which is fairly small given the difficulty of testing the assumptions of the laser scan dataset and accessing the system *in situ*.

Acknowledgments The author acknowledges the many and valuable contributions of the EQS group for guiding the laser scan dataset analysis; the AMD group and especially Horst Friedsam for assistance with all surveys; the field trolley group for support and allowing me to use their system; and John Nadjzion for repeatedly accommodating my machining requests within his tight schedule.

Appendices

A Survey of kicker plates

As shown in Fig. 20, the dataset collected by the VCNL4010 sensors includes a survey of the kicker plates. Fig. 25 [21] focuses on the VCNL measurements around the region of the kickers, where the three main data islands correspond to the three kicker plates. The edges of the quadrupole plates Q1L and Q2S are also apparent. Note that we only use the data from the trolley moving downstream through the kickers. For each quad plate we had used data from two separate passes of the trolley, moving upstream and downstream. But for the first pass through the kickers moving upstream, we were being careful and moving the trolley in small intervals to ensure that no interaction occurs between the sensors and the plates. As a result that data is now difficult to match with the exact azimuthal location that is being sampled, and will not be used.

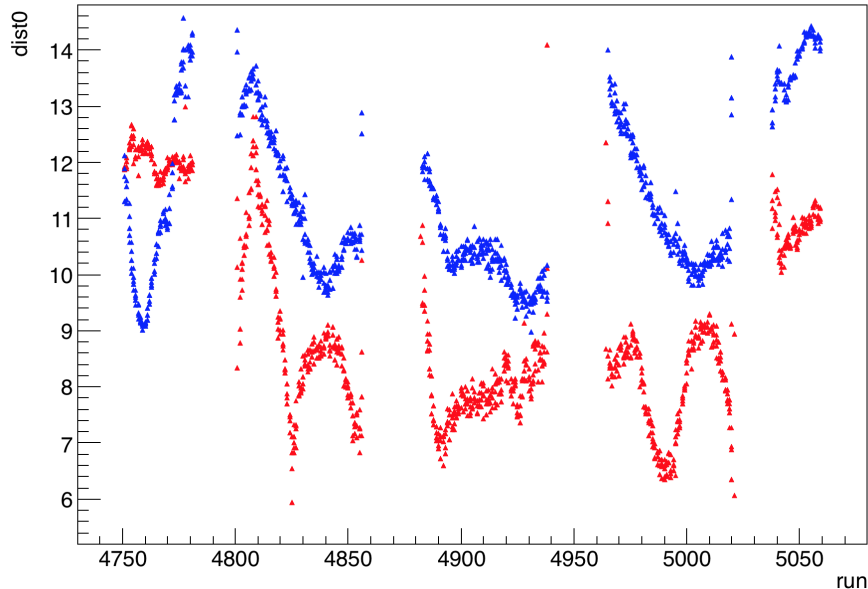


Figure 25: The raw data collected by the VCNL4010 sensors around the region of the kicker plates, plotted versus run time.

The proximity distance measurement in Fig. 25 relies on the sensor calibration. As before we extract the trolley rails location from the existing AMD data, separately for each kicker plate. Finally we use the same "geometric factors" for the VCNL sensors that we extracted from fitting to the known quad plates, which yielded overall very good agreement between the VCNL measurement and other surveys.

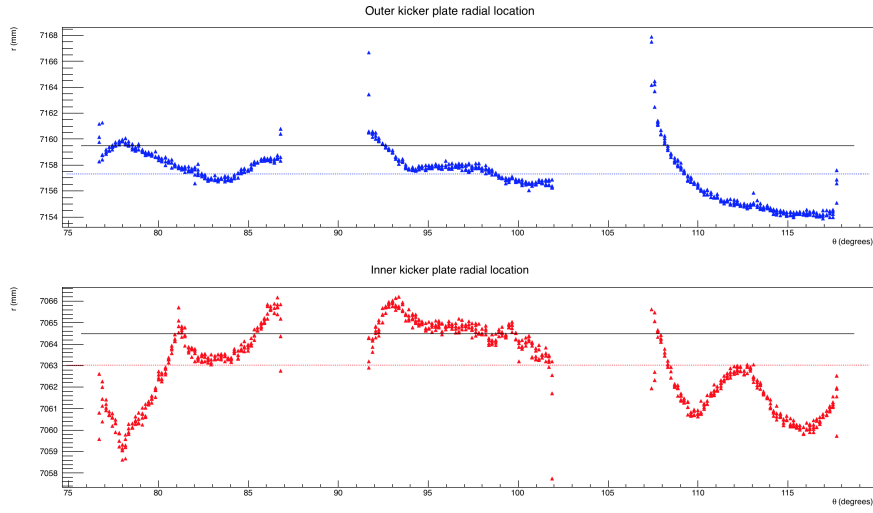


Figure 26: The location of all three inner and outer kicker plates, plotted versus azimuth. Fits to the VCNL sensor data are shown as dashed lines for each plate. The solid black lines mark the ideal plate locations.

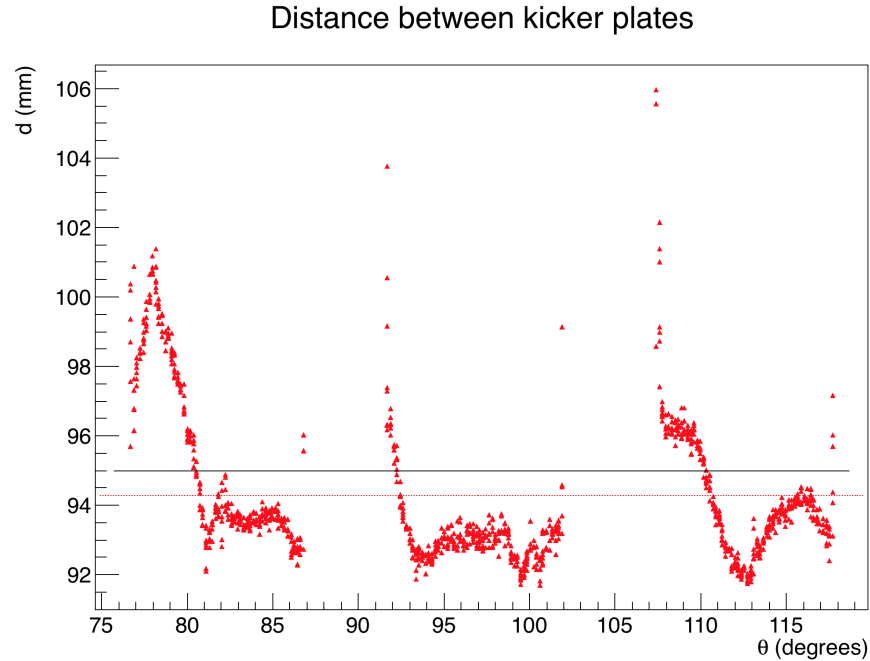


Figure 27: The distance between inner and outer plates of the three kickers.

The location of the inner and outer kicker plates is plotted in Fig. 26. The ideal position of the plates is ± 47.5 mm from $r_0=7112$ mm, shown as a solid black line in the figure. Fits for the average location over all three kickers are shown as dashed lines. It is evident that both plates are more inwards than designed, on average.

The most inwards location of all outer plates is at the downstream end of K3. It is then no surprise that the interaction with the outer sensor occurred there. It was unfortunate that the sensor fixture happened to be misaligned outwards in that run. The distance between opposite kicker plates is plotted in Fig. 27.

Table 7: Average locations of kicker plates and offset from ideal. All values in mm.

		VCNL survey	Offset from design
K1	Inner plate	7062.88	-1.62
	Outer plate	7158.19	-1.31
	Out-In	95.36	0.36
K2	Inner plate	7064.61	0.11
	Outer plate	7157.77	-1.73
	Out-In	93.22	-1.78
K3	Inner plate	7061.61	-2.89
	Outer plate	7155.77	-3.73
	Out-In	94.27	-0.73
Average over all plates	Inner plate	7063.03	-1.47
	Outer plate	7,157.24	-2.26
	Out-In	94.28	-0.72

Values for plate locations and distance between plates averaged over all three kickers are listed in Table 7. It confirms that the average plate locations are inwards by ~ 2 mm relative to the design position. The distance between the plates is also smaller than designed. These offsets from ideal are generally larger than we saw on the quad plates, where they are more tightly controlled. The reason is that a stored muon may pass thousands of times through a field of a quad plate in a single fill, whereas it should be kicked only once, ideally. Therefore alignment is a much less important consideration for the kicker system.

References

- [1] Y. K. Semertzidis et al. The Brookhaven muon (g-2) storage ring high voltage quadrupoles. *Nucl. Instrum. Meth.*, A503:458–484, 2003.
- [2] J. Grange et al. Muon (g-2) Technical Design Report. 2015.
- [3] J. Grange and W. Morse. E989 Note 57: ES Quadrupole Specs vs N. Muon g-2 DocDB-3632.

- [4] A. Fienberg. *Measuring the Precession Frequency in the E989 Muon g-2 Experiment*. PhD thesis, University of Washington, 2019. Muon g-2 DocDB-16264.
- [5] O. Zhanibek and Y. K. Semertzidis. E field correction uncertainties due to quad misalignment for FNAL E989 Muon g-2 experiment.
- [6] Non-contact displacement Capacitec short form manual. <http://www.process-controls.com/intertechnology/Capacitec/pdfs/ShortForm.pdf>.
- [7] W. Wu et al. Using Capacitec to Investigate Quad Plate Alignment. Muon g-2 DocDB-3709.
- [8] W. Wu et al. E989 note 116: Electrostatic quadrupoles: Plate alignment. Muon g-2 DocDB-8036.
- [9] API iProbe 360. <https://apisensor.com/products/3d-laser-tracker-systems/i-360/>.
- [10] H. Friedsam. Alignment results 22Feb17. Muon g-2 DocDB-5955.
- [11] M. Kargiantoulakis. Status of quad alignment studies. Muon g-2 DocDB-12906.
- [12] J. Grange. Trolley alignment data from horst. Muon g-2 UW elog-386.
- [13] M. Kargiantoulakis. ESQ Keyence measurement update. Muon g-2 DocDB-14776.
- [14] M. Kargiantoulakis. Quads survey through flange. Muon g-2 DocDB-15679.
- [15] VCNL4010 Product Information from Vishay Semiconductors. <https://www.vishay.com/optical-sensors/list/product-83462/>.
- [16] M. Kargiantoulakis. Quad alignment measurements update. Muon g-2 DocDB-14547.
- [17] M. Kargiantoulakis. Trolley cable tension analysis for dropped components. Muon g-2 DocDB-14938.
- [18] M. Kargiantoulakis. Quads survey from sensors mounted on trolley. Muon g-2 DocDB-15733.
- [19] M. Kargiantoulakis. Location and uncertainty of ESQ plates. Muon g-2 DocDB-16324.
- [20] H. Nguyen. Effect of Q1 Outer Mylar Waviness on Beam Dynamics. Muon g-2 DocDB-4586.
- [21] M. Kargiantoulakis. Survey of kicker plates with proximity sensors on trolley. Muon g-2 DocDB-16976.